

Received 24 May 2018  
Accepted 6 June 2018

Edited by D.-J. Xu, Zhejiang University (Yuquan Campus), China

**Keywords:** oxoanion salt; crystal structure; organic dinitrate; Hirshfeld surface; fingerprint plots; energy framework.

**CCDC reference:** 1847743

**Supporting information:** this article has supporting information at journals.iucr.org/e

# Crystal structure, Hirshfeld surface analysis and energy framework calculation of the first oxoanion salt containing 1,3-cyclohexanebis(methylammonium): [3-(azaniumylmethyl)cyclohexyl]-methanaminium dinitrate

Hammouda Chebbi,<sup>a,b\*</sup> Samia Mezrigui,<sup>a</sup> Meriam Ben Jomaa<sup>a</sup> and Mohamed Faouzi Zid<sup>a</sup>

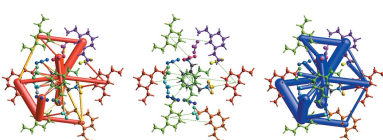
<sup>a</sup>University of Tunis El Manar, Faculty of Sciences of Tunis, Laboratory of Materials, Crystal Chemistry and Applied Thermodynamics, 2092 El Manar II, Tunis, Tunisia, and <sup>b</sup>University of Tunis, Preparatory Institute for Engineering Studies of Tunis, Street Jawaher Lel Nehru, 1089 Montfleury, Tunis, Tunisia. \*Correspondence e-mail: chebhamouda@yahoo.fr

The title salt,  $C_8H_{20}N_2^{2+}\cdot 2NO_3^-$ , was obtained by a reaction between 1,3-cyclohexanebis(methylamine) and nitric acid. The cyclohexane ring of the organic cation is in a chair conformation with the methylammonium substituents in the equatorial positions and the two terminal ammonium groups in a *trans* conformation. In the crystal, mixed cation–anion layers lying parallel to the (010) plane are formed through N–H···O hydrogen-bonding interactions; these layers are formed by infinite undulating chains running parallel to the [001] direction. The overall intermolecular interactions involved in the structure were quantified and fully described by Hirshfeld surface analysis. In addition, energy-framework calculations were used to analyse and visualize the three-dimensional topology of the crystal packing. The electrostatic energy framework is dominant over the dispersion energy framework.

## 1. Chemical context

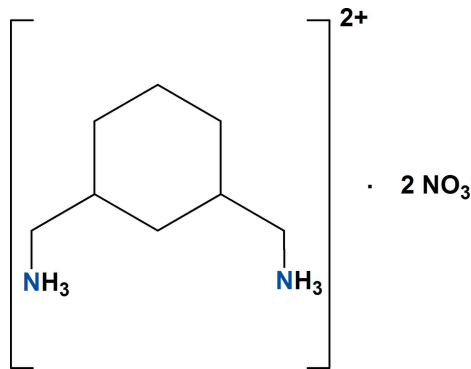
The design of new organic–inorganic hybrid ionic materials is of current interest for various applications, particularly in the areas of crystal engineering, supramolecular chemistry and materials science (Kimizuka & Kunitake, 1996; Mitzi *et al.*, 1999; Bonhomme & Kanatzidis, 1998; Wachhold & Kanatzidis, 2000), and also for optical semiconductor materials (Kagan *et al.*, 1999; Li *et al.*, 2008). Among these hybrid compounds, organic nitrates are particularly interesting for their multiple applications including as catalytic precursors of numerous reactions, in biological treatment systems or as pharmaceutical products (Brandán, 2012*a,b*, 2015; Castillo *et al.*, 2011; Torfgård & Ahlner, 1994).

1,3-Cyclohexanebis(methylamine) (CHMA) is used industrially as a hardener for epoxy resins, a raw material for the production of polyamides and isocyanates, a rubber chemical for paper-processing agents, in fiber treatment agents and in cleaning agents (Pham & Marks, 2012). It can also be used as an effective new cross-linking agent for the chemical modification of polyimide membranes (Shao *et al.*, 2005). We have previously reported on the use of the 1,3-cyclohexanebis(methylammonium) cation in the syntheses of organic–inorganic hybrid ionic complexes (Huo *et al.*, 1992; Yang *et al.*, 2008), but to the best of our knowledge there are no reported salt forms containing an oxoanion and 1,3-cyclohexanebis(methylammonium).



OPEN ACCESS

In a continuation of our recent studies of new hybrid compounds containing an organic cation and an inorganic oxoanion such as  $\text{CrO}_4^{2-}$  (Chebbi *et al.*, 2000; Chebbi & Driss, 2001, 2002*a,b*, 2004),  $\text{Cr}_2\text{O}_7^{2-}$  (Chebbi *et al.*, 2016; Ben Smail *et al.*, 2017),  $\text{NO}_3^-$  (Chebbi *et al.*, 2014) and  $\text{ClO}_4^-$  (Chebbi *et al.*, 2017; Ben Jomaa *et al.*, 2018), we report in this work the crystal structure, Hirshfeld surface analysis and energy-framework calculations for a new organic nitrate,  $(\text{C}_8\text{H}_{20}\text{N}_2)[\text{NO}_3]_2$  (I).



## 2. Structural commentary

The title compound crystallizes with one 1,3-cyclohexane-bis(methylammonium) dication,  $(\text{CHMA})^{2+}$ , and two nitrate anions in the asymmetric unit (Fig. 1). An EDX spectrum confirming the presence of C, N, and O is shown in Fig. 2.

All atoms of the nitrate anion are coplanar with the N–O bond distances varying between 1.218 (4) and 1.250 (4) Å. The O–N–O angles are in the range of 118.8 (4)–121.1 (4)°. These bond lengths and angles are in good agreement with those observed in similar compounds (Blerk & Kruger, 2009; Gatfaoui *et al.*, 2017; Hakiri *et al.*, 2018). The cyclohexane ring of the organic cation adopts a chair conformation with the methylammonium substituents in the equatorial positions and the two terminal ammonium groups in a *trans* conformation (Fig. 1). The same *trans* conformation has been observed in

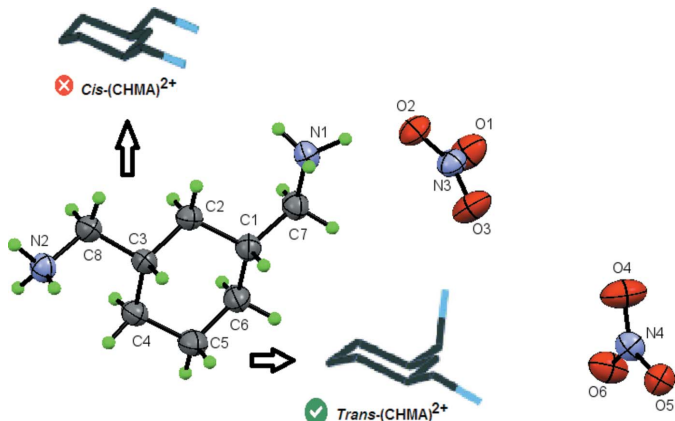


**Figure 1**

The asymmetric unit of (I), showing the atom-labeling scheme, displacement ellipsoids at the 30% probability level and the two configurations, cis and trans, of  $(\text{CHMA})^{2+}$ .

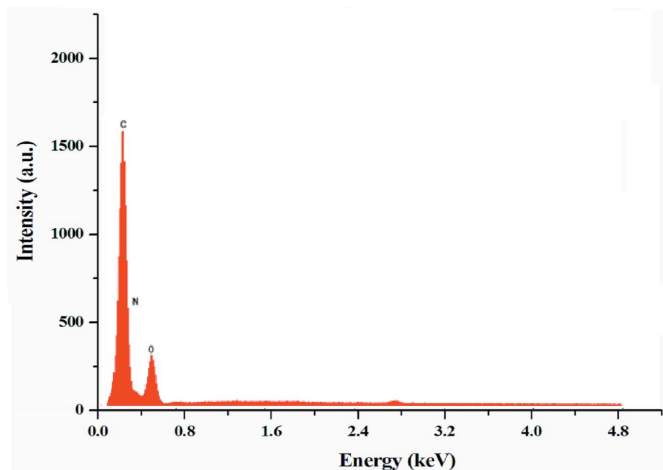


**Figure 2**

The EDX spectrum of (I), showing the presence of C, N, and O.

other compounds with this organic cation (Zhao *et al.*, 2008). Examination of the C–C (N) distances and C–C–C (N) angles in the  $(\text{CHMA})^{2+}$  dication shows no significant difference from those in other organic materials associated with the same organic groups (Huo *et al.*, 1992; Yang *et al.*, 2008).

## 3. Supramolecular features

In the crystal, the  $(\text{CHMA})^{2+}$  cations and nitrate anions are linked by N–H···O hydrogen bonds into infinite layers parallel to the *ac* plane (Fig. 3). Each layer is formed of infinite undulating chains running parallel to the [001] direction, further extended into an overall two-dimensional supramolecular network structure (Fig. 4). As seen in Table 1, all of the hydrogen atoms bonded to the amine group of  $(\text{CHMA})^{2+}$  dication contribute to the formation of N–H···O hydrogen bonds with the nitrate anions. The  $-\text{N}(1,2)\text{H}_3^+$  groups of the organic cations, which act as donors to the  $\text{N}(3,4)\text{O}_3^-$  anions generate  $R_1^2(3)$  dimeric rings. The propagation of these dimers produces infinite undulating chains running parallel to the [001] direction (Fig. 5). The interconnection of two adjacent undulating chains leads to the generation of another two

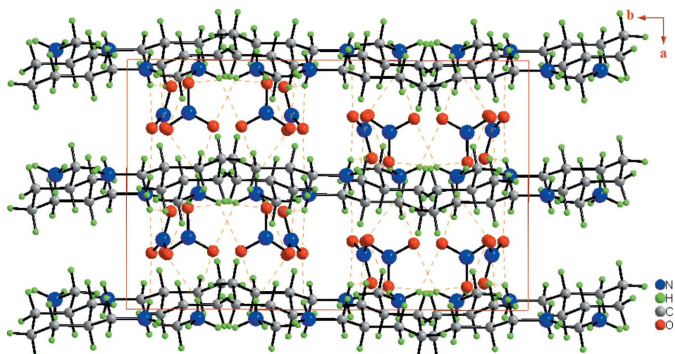


**Figure 3**

Structure of (I) viewed along the [001] direction, showing the infinite layers parallel to the *ac* plane. The N–H···O hydrogen bonds are shown as orange dashed lines.

**Table 1**  
Hydrogen-bond geometry ( $\text{\AA}$ ,  $^\circ$ ).

$D-\text{H}\cdots A$	$D-\text{H}$	$\text{H}\cdots A$	$D\cdots A$	$D-\text{H}\cdots A$
N1—H1A $\cdots$ O2 <sup>i</sup>	0.87 (4)	2.22 (4)	3.084 (6)	169 (4)
N1—H1A $\cdots$ O3 <sup>i</sup>	0.87 (4)	2.36 (4)	3.013 (5)	132 (3)
N1—H1B $\cdots$ O4 <sup>ii</sup>	0.95 (4)	2.59 (4)	3.187 (6)	121 (3)
N1—H1B $\cdots$ O5 <sup>ii</sup>	0.95 (4)	1.87 (4)	2.818 (5)	172 (3)
N1—H1C $\cdots$ O2 <sup>iii</sup>	0.87 (5)	2.12 (5)	2.939 (6)	157 (4)
N2—H2D $\cdots$ O4 <sup>iv</sup>	0.77 (4)	2.48 (4)	3.142 (6)	145 (4)
N2—H2D $\cdots$ O6 <sup>iv</sup>	0.77 (4)	2.19 (4)	2.899 (6)	153 (4)
N2—H2E $\cdots$ O1 <sup>iv</sup>	0.99 (4)	2.46 (4)	3.178 (6)	130 (3)
N2—H2E $\cdots$ O3 <sup>iv</sup>	0.99 (4)	1.88 (4)	2.858 (5)	173 (4)
N2—H2F $\cdots$ O5 <sup>v</sup>	0.96 (6)	2.05 (6)	2.967 (5)	159 (5)
N2—H2F $\cdots$ O6 <sup>v</sup>	0.96 (6)	2.23 (6)	3.016 (6)	139 (4)

Symmetry codes: (i)  $-x + 1, -y, -z + 1$ ; (ii)  $-x + \frac{3}{2}, -y, z + \frac{1}{2}$ ; (iii)  $-x + \frac{1}{2}, -y, z + \frac{1}{2}$ ; (iv)  $x, y, z + 1$ ; (v)  $x - \frac{1}{2}, -y - \frac{1}{2}, -z + 1$ .

hexameric  $R_6^3(12)$  and  $R_6^4(14)$  ring motifs. Thus, the three types of  $R_1^2(3)$ ,  $R_6^3(12)$  and  $R_6^4(14)$  rings are alternately linked into infinite layers parallel to the  $ac$  plane (Fig. 6).

#### 4. Hirshfeld surface analysis and energy framework calculations

The Hirshfeld surfaces (Spackman & Jayatilaka, 2009) and their relative 2D fingerprint plots (Spackman & McKinnon, 2002; Parkin *et al.*, 2007; Rohl *et al.*, 2008)) were drawn using *CrystalExplorer 3.1* (Wolff *et al.*, 2012). The quantifying and decoding of the intermolecular contacts in the crystal packing are visualized using  $d_{\text{norm}}$  (normalized contact distance) and 2D fingerprint plots, respectively. The dark-red spots on the  $d_{\text{norm}}$  surface arise as a result of short interatomic contacts, while the other intermolecular interactions appear as light-red spots.  $d_i$  (inside) and  $d_e$  (outside) represent the distances to the Hirshfeld surface from the nuclei, with respect to the relative van der Waals radii. The proportional contribution of the contacts over the surface is visualized by the color gradient (blue to red) in the fingerprint plots.

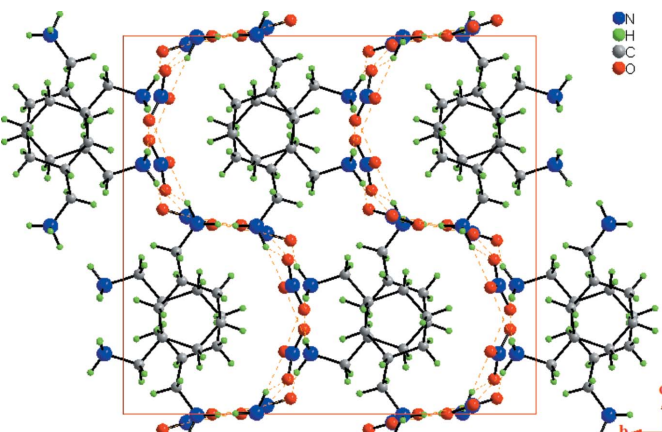


**Figure 4**  
Unit-cell contents for (I) shown in projection down the  $a$  axis, showing the infinite undulating chains. The orange dotted lines indicate  $\text{N}-\text{H}\cdots\text{O}$  hydrogen bonds.

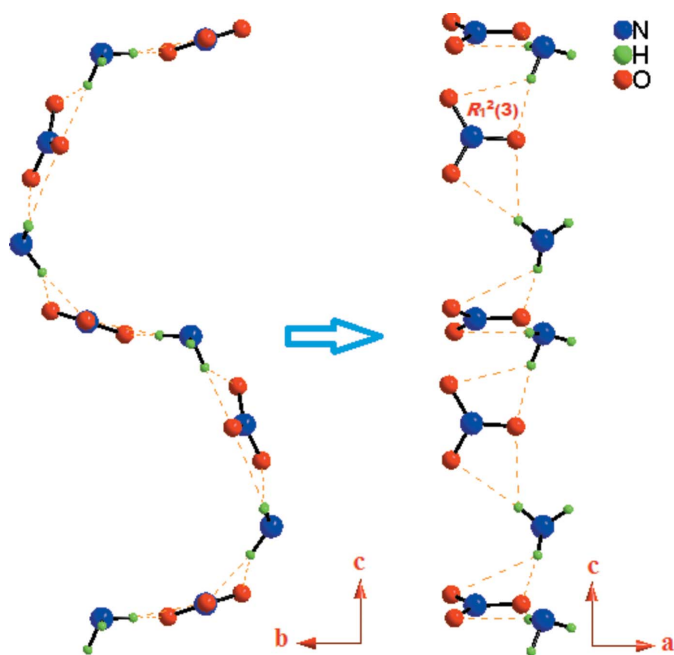


**Figure 5**  
A view showing the  $R_1^2(3)$  motif built by  $\text{N}-\text{H}\cdots\text{O}$  hydrogen bonds in the undulating chain. C and H atoms not involved in the intermolecular interactions (dashed lines) have been omitted for clarity.

The Hirshfeld surface mapped over  $d_{\text{norm}}$  in the range 0.0620 to 0.9660 a.u. is illustrated in Fig. 7. Information regarding the intermolecular interactions, visible as spots on the Hirshfeld surface (Fig. 7), is summarized in Table 1. For instance, the distinct circular depressions (red spots) are due to the  $\text{N}-\text{H}\cdots\text{O}$  contacts, whereas the white spots are due to  $\text{H}\cdots\text{H}$  contacts.

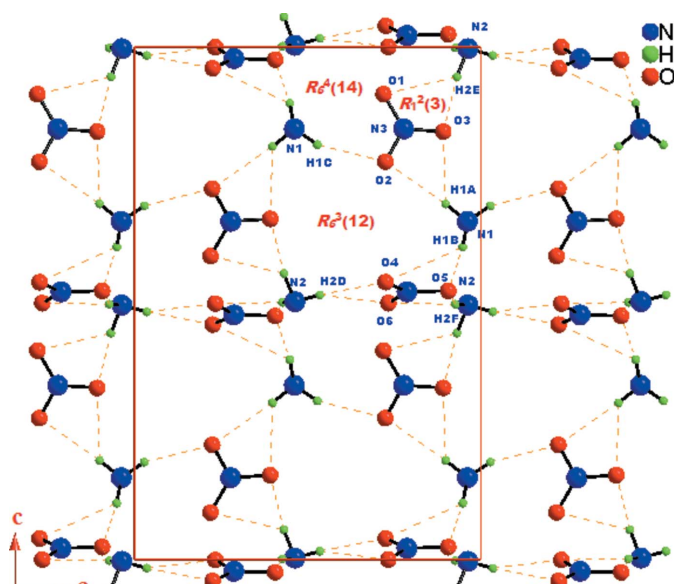


**Figure 6**  
A view of the supramolecular layer in the  $ac$  plane of (I), showing the formation of the  $R_1^2(3)$ ,  $R_6^3(12)$  and  $R_6^4(14)$  motifs. C and H atoms not involved in hydrogen bonds (orange dashed lines) have been omitted for clarity.

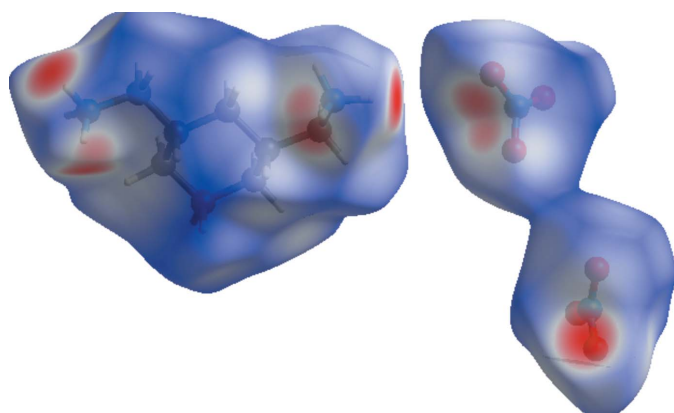


Figure 7

Hirshfeld surface around the constituents of (I) coloured according to  $d_{\text{norm}}$ . The surface is shown as transparent to allow visualization of the orientation and conformation of the functional groups.

The intermolecular interactions present in the structure are also visible on the two-dimensional fingerprint plot, which can be decomposed to quantify the individual contributions of each intermolecular interaction involved in the structure. The H $\cdots$ O/O $\cdots$ H contacts associated with N—H $\cdots$ O hydrogen bonding appear to be the major contributor to the crystal packing (68.8%); these contacts are represented by the spikes in the top-left ( $d_e > d_i$ , H $\cdots$ O, 31.3%) and bottom-right ( $d_e < d_i$ , O $\cdots$ H, 37.5%) regions of the related plots in Fig. 8a. Interactions of the type H $\cdots$ H appear in the middle of the scattered points in the fingerprint plots; they comprise 24.6%

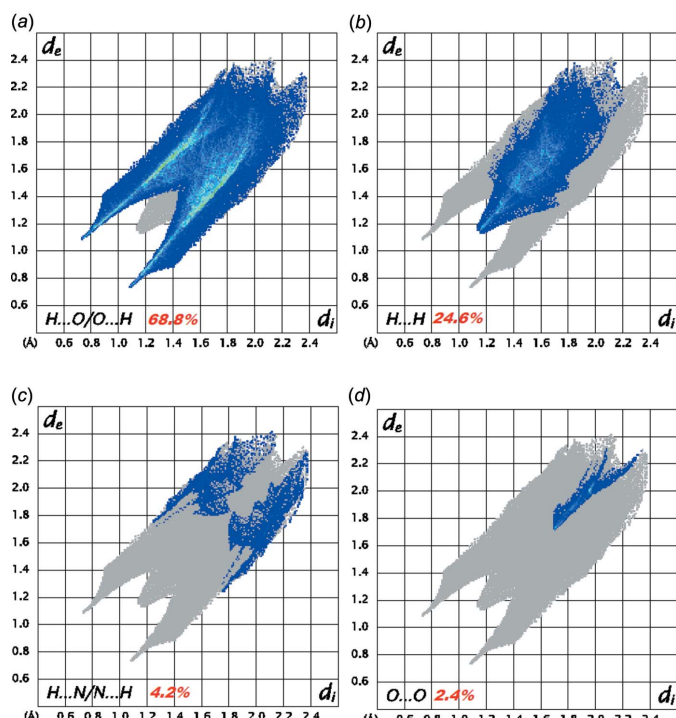


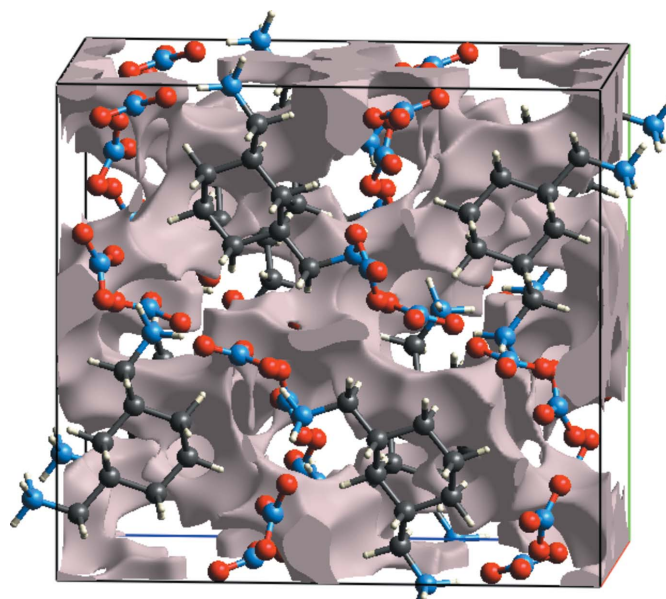
Figure 8

Two-dimensional fingerprint plots for (I) showing contributions from different contacts: (a) H $\cdots$ O/O $\cdots$ H, (b) H $\cdots$ H, (c) H $\cdots$ N/N $\cdots$ H and (d) O $\cdots$ O.

of the entire surface (Fig. 8b). The forceps-like tips in the region  $d_e + d_i \approx 3$  Å of the fingerprint plot (Fig. 8c) represent a significant H $\cdots$ N/N $\cdots$ H contribution, covering 4.2% of the total Hirshfeld surface of (I). The O $\cdots$ O contacts, which represent only 2.4% of the Hirshfeld surface, Fig. 8d, are extremely impoverished in the crystal (enrichment ratio  $E_{\text{OO}} = 0.17$ ; Jelsch *et al.*, 2014), as the oxygen atoms bound to nitrogen and the NO<sub>3</sub> group as a whole are electronegative, therefore the O $\cdots$ O contacts are electrostatically repulsive.

Fig. 9 shows the voids (Wolff *et al.*, 2012) in the crystal structure of (I). These are based on the sum of spherical atomic electron densities at the appropriate nuclear positions (procryystal electron density). The crystal-void calculation (results under 0.002 a.u. isovalue) shows the void volume of title compound to be of the order of 469.14 Å<sup>3</sup> and surface area in the order of 1334.82 Å<sup>2</sup>. With the porosity, the calculated void volume of (I) is 17%. There are no large cavities. We note that the electron-density isosurfaces are not completely closed around the components, but are open at those locations where interspecies approaches are found, *e.g.* N—H $\cdots$ O.

The crystallographic information file (crystal geometry and hydrogen bond distances to 1.083 Å) was used as input to *CrystalExplorer 17* (Turner *et al.*, 2017) and the intermolecular interaction energies were calculated for the energy-framework analysis. This calculation is estimated from a single-point molecular wavefunction at B3LYP/6-31G(d,p). A cluster of radius 3.8 Å was generated around the molecule and the energy calculation was performed. The neighbouring molecules (density matrices) are generated within this shell by applying crystallographic symmetry operations with respect to the central molecule (density matrix). The interaction energy is broken down as  $E_{\text{tot}} = k_{\text{ele}}E'_{\text{ele}} + k_{\text{pol}}E'_{\text{pol}} + k_{\text{dis}}E'_{\text{dis}} + k_{\text{rep}}E'_{\text{rep}}$  where the  $k$  values are scale factors,  $E'_{\text{ele}}$  represents the elec-

Figure 9  
Void plot for (I).

**Table 2**  
Interaction energies.

N refers to the number of molecules with an  $R$  molecular centroid-to-centroid distance ( $\text{\AA}$ ). Energies are in  $\text{kJ mol}^{-1}$ .

N	Symop	R	$E'_{\text{ele}}$	$E'_{\text{pol}}$	$E'_{\text{dis}}$	$E'_{\text{rep}}$	$E_{\text{tot}}$
2	$-x, -y + \frac{1}{2}, z + \frac{1}{2}$	8.51	-63.9	-50.6	-6.3	5.4	-107.1
1	$-x, -y, -z$	9.69	32.1	-42.9	-4.6	1.8	-0.7
2	$x, y + \frac{1}{2}, -z + \frac{1}{2}$	8.86	0.0	-53.8	0.0	0.0	-39.8
2	$x + \frac{1}{2}, -y + \frac{1}{2}, z$	5.33	-23.1	-75.4	-20.1	14.1	-89.0
1	$x + \frac{1}{2}, -y + \frac{1}{2}, z$	5.60	-21.5	-50.6	-6.3	2.1	-64.4
1	$x + \frac{1}{2}, -y + \frac{1}{2}, z$	5.77	11.3	-14.6	-0.5	0.0	0.7
1	$x + \frac{1}{2}, -y + \frac{1}{2}, z$	5.33	-44.5	-18.9	-0.8	0.0	-61.8
1	$-x, -y, -z$	7.97	-128.4	-53.8	-4.3	0.2	-179.2
1	$-x, -y, -z$	6.43	-9.8	-18.9	-0.8	0.0	-25.0

Scale factors used to determine  $E_{\text{tot}}$ :  $k_{\text{ele}} = 1.057$ ,  $k_{\text{pol}} = 0.740$ ,  $k_{\text{dis}} = 0.871$ ,  $k_{\text{rep}} = 0.618$  (Mackenzie *et al.*, 2017).

trostatic component,  $E'_{\text{pol}}$  the polarization energy,  $E'_{\text{dis}}$  the dispersion energy, and  $E'_{\text{rep}}$  the exchange-repulsion energy (Turner *et al.*, 2014; Mackenzie *et al.*, 2017).

Table 2 shows the results of the interaction energies calculations. The results are represented graphically in Fig. 10 as framework energy diagrams. The molecular pair-wise interaction energies calculated for the construction of energy frameworks are used to evaluate the net interaction energies. The total interaction energies are electrostatic ( $E'_{\text{ele}} = -247.8 \text{ kJ mol}^{-1}$ ), polarization ( $E'_{\text{pol}} = -379.5 \text{ kJ mol}^{-1}$ ), dispersion ( $E'_{\text{dis}} = -43.7 \text{ kJ mol}^{-1}$ ), repulsion ( $E'_{\text{rep}} = 23.6 \text{ kJ mol}^{-1}$ ), and total interaction energy ( $E_{\text{tot}} = -566.3 \text{ kJ mol}^{-1}$ ). The electrostatic energy framework is dominant over the dispersion energy framework (Fig. 10).

## 5. Synthesis and crystallization

1,3-Cyclohexanebis(methylamine) (1 mmol) was dissolved in water (10 mL) and nitric acid (2 mmol in 10 mL of water). The resulting solution was stirred for 3 h, filtered and then left to stand at room temperature. Colorless crystals were obtained after five days by slow evaporation.

**Table 3**  
Experimental details.

Crystal data	$C_8H_{20}N_2^{2+}\cdot 2NO_3^-$
Chemical formula	
$M_r$	268.28
Crystal system, space group	Orthorhombic, $Pbca$
Temperature (K)	293
$a, b, c$ ( $\text{\AA}$ )	10.475 (4), 16.884 (4), 15.514 (2)
$V$ ( $\text{\AA}^3$ )	2743.8 (13)
$Z$	8
Radiation type	Mo $K\alpha$
$\mu$ ( $\text{mm}^{-1}$ )	0.11
Crystal size (mm)	0.52 $\times$ 0.40 $\times$ 0.15
Data collection	
Diffractometer	Enraf–Nonius CAD-4
Absorption correction	$\psi$ scan (North <i>et al.</i> , 1968)
$T_{\min}, T_{\max}$	0.946, 1.000
No. of measured, independent and observed [ $I > 2\sigma(I)$ ] reflections	3798, 2980, 991
$R_{\text{int}}$	0.036
( $\sin \theta/\lambda$ ) <sub>max</sub> ( $\text{\AA}^{-1}$ )	0.638
Refinement	
$R[F^2 > 2\sigma(F^2)]$ , $wR(F^2)$ , $S$	0.062, 0.173, 0.98
No. of reflections	2980
No. of parameters	187
H-atom treatment	H atoms treated by a mixture of independent and constrained refinement
$\Delta\rho_{\text{max}}, \Delta\rho_{\text{min}}$ ( $e \text{\AA}^{-3}$ )	0.17, -0.13

Computer programs: CAD-4 EXPRESS (Duisenberg, 1992; Maciček & Yordanov, 1992), XCAD4 (Harms & Wocadlo, 1995), SHELXS97 (Sheldrick, 2008), SHELXL2014 (Sheldrick, 2015), DIAMOND (Brandenburg, 2006), Mercury (Macrae *et al.*, 2006), WinGX (Farrugia, 2012) and publCIF (Westrip, 2010).

## 6. Refinement

Crystal data, data collection and structure refinement details are summarized in Table 3. All C-bound hydrogen atoms were included in calculated positions with C—H = 0.98 (CH group) or 0.97  $\text{\AA}$  (methylene) and allowed to ride, with  $U_{\text{iso}}(\text{H}) = 1.2U_{\text{eq}}(\text{C})$ . N-bound H atoms were located in difference-Fourier maps and freely refined.

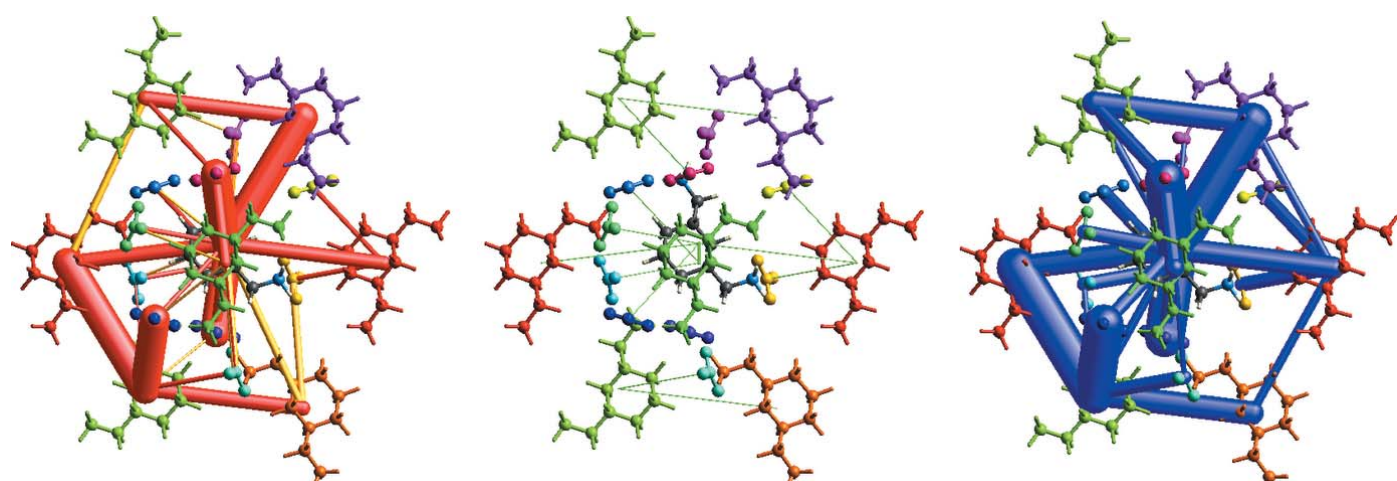


**Figure 10**  
Energy framework diagram for separate electrostatic (left, red) and dispersion (middle, green) components of (I) and the total interaction energy (right, blue). The energy factor scale is 60 and the cut-off is  $5.00 \text{ kJ mol}^{-1}$ .

## Acknowledgements

The authors are grateful to Dr R. Ben Smail, Carthage University, Preparatory Institute for Engineering Studies of Nabeul, for fruitful discussions.

## References

- Ben Jomaa, M., Chebbi, H., Fakhar Bourguiba, N. & Zid, M. F. (2018). *Acta Cryst. E* **74**, 91–97.
- Ben Smail, R., Chebbi, H., Srinivasan, B. R. & Zid, M. F. (2017). *J. Struct. Chem.* **58**, 724–733.
- Blerk, C. van & Kruger, G. J. (2009). *Acta Cryst. E* **65**, o1008.
- Bonhomme, F. & Kanatzidis, M. G. (1998). *Chem. Mater.* **10**, 1153–1159.
- Brandán, S. A. (2012a). *Nitrate: occurrence, characteristics and health considerations*. Edited Collection. Hauppauge, New York: Nova Science Publishers.
- Brandán, S. A. (2012b). *Structural and vibrational study of the chromyl chlorosulfate, fluorosulfate, and nitrate compounds*. Dordrecht: Springer.
- Brandán, S. A. (2015). *Descriptors, structural and spectroscopic properties of heterocyclic derivatives of importance for the health and the environment*. Edited Collection. Hauppauge, New York: Nova Science Publishers.
- Brandenburg, K. (2006). DIAMOND. Crystal Impact GbR, Bonn, Germany.
- Castillo, M. V., Romano, E., Lanús, H. E., Díaz, S. B., Ben Altabef, A. & Brandán, S. A. (2011). *J. Mol. Struct.* **994**, 202–208.
- Chebbi, H., Ben Smail, R. & Zid, M. F. (2014). *Acta Cryst. E* **70**, o642.
- Chebbi, H., Ben Smail, R. & Zid, M. F. (2016). *J. Struct. Chem.* **57**, 632–635.
- Chebbi, H., Boumakhla, A., Zid, M. F. & Guesmi, A. (2017). *Acta Cryst. E* **73**, 1453–1457.
- Chebbi, H. & Driss, A. (2001). *Acta Cryst. C* **57**, 1369–1370.
- Chebbi, H. & Driss, A. (2002a). *Acta Cryst. E* **58**, m147–m149.
- Chebbi, H. & Driss, A. (2002b). *Acta Cryst. E* **58**, m494–m496.
- Chebbi, H. & Driss, A. (2004). *Acta Cryst. E* **60**, m904–m906.
- Chebbi, H., Hajem, A. A. & Driss, A. (2000). *Acta Cryst. C* **56**, e333–e334.
- Duisenberg, A. J. M. (1992). *J. Appl. Cryst.* **25**, 92–96.
- Farrugia, L. J. (2012). *J. Appl. Cryst.* **45**, 849–854.
- Gatfaoui, S., Mezni, A., Roisnel, T. & Marouani, H. (2017). *J. Mol. Struct.* **1139**, 52–59.
- Hakiri, R., Ameur, I., Abid, S. & Derbel, N. (2018). *J. Mol. Struct.* **1164**, 468–492.
- Harms, K. & Wocadlo, S. (1995). XCAD4. University of Marburg, Germany.
- Huo, Q., Xu, R., Li, S., Ma, Z., Thomas, J. M., Jones, R. H. & Chippindale, A. M. (1992). *J. Chem. Soc. Chem. Commun.* pp. 875–876.
- Jelsch, C., Ejsmont, K. & Huder, L. (2014). *IUCrJ*, **1**, 119–128.
- Kagan, C. R., Mitzi, D. B. & Dimitrakopoulos, C. D. (1999). *Science*, **286**, 945–947.
- Kimizuka, N. & Kunitake, T. (1996). *Adv. Mater.* **8**, 89–91.
- Li, H.-H., Chen, Z.-R., Cheng, L.-C., Liu, J.-B., Chen, X.-B. & Li, J.-Q. (2008). *Cryst. Growth Des.* **8**, 4355–4358.
- Maciček, J. & Yordanov, A. (1992). *J. Appl. Cryst.* **25**, 73–80.
- Mackenzie, C. F., Spackman, P. R., Jayatilaka, D. & Spackman, M. A. (2017). *IUCrJ*, **4**, 575–587.
- Macrae, C. F., Edgington, P. R., McCabe, P., Pidcock, E., Shields, G. P., Taylor, R., Towler, M. & van de Streek, J. (2006). *J. Appl. Cryst.* **39**, 453–457.
- Mitzi, D. B., Prikas, M. T. & Chondroudis, K. (1999). *Chem. Mater.* **11**, 542–544.
- North, A. C. T., Phillips, D. C. & Mathews, F. S. (1968). *Acta Cryst. A* **24**, 351–359.
- Parkin, A., Barr, G., Dong, W., Gilmore, C. J., Jayatilaka, D., McKinnon, J. J., Spackman, M. A. & Wilson, C. C. (2007). *CrystEngComm*, **9**, 648–652.
- Pham, H. Q. & Marks, M. J. (2012). *Ullmann's Encyclopedia of Industrial Chemistry*. Weinheim: Wiley-VCH.
- Rohl, A. L., Moret, M., Kaminsky, W., Claborn, K., McKinnon, J. J. & Kahr, B. (2008). *Cryst. Growth Des.* **8**, 4517–4525.
- Shao, L., Chung, T. S., Goh, S. H. & Pramoda, K. P. (2005). *J. Membr. Sci.* **267**, 78–89.
- Sheldrick, G. M. (2008). *Acta Cryst. A* **64**, 112–122.
- Sheldrick, G. M. (2015). *Acta Cryst. C* **71**, 3–8.
- Spackman, M. A. & Jayatilaka, D. (2009). *CrystEngComm*, **11**, 19–32.
- Spackman, M. A. & McKinnon, J. J. (2002). *CrystEngComm*, **4**, 378–392.
- Torfgård, K. E. & Ahlner, J. (1994). *Cardiovasc. Drug. Ther.* **8**, 701–717.
- Turner, M. J., Grabowsky, S., Jayatilaka, D. & Spackman, M. A. (2014). *J. Phys. Chem. Lett.* **5**, 4249–4255.
- Turner, M. J., McKinnon, J. J., Wolff, S. K., Grimwood, D. J., Spackman, P. R., Jayatilaka, D. & Spackman, M. A. (2017). *CrystalExplorer 17*. University of Western Australia.
- Wachhold, M. & Kanatzidis, M. G. (2000). *Chem. Mater.* **12**, 2914–2923.
- Westrip, S. P. (2010). *J. Appl. Cryst.* **43**, 920–925.
- Wolff, S. K., Grimwood, D. J., McKinnon, J. J., Turner, M. J., Jayatilaka, D. & Spackman, M. A. (2012). *CrystalExplorer 3.1*. University of Western Australia.
- Yang, Y., Zhao, Y., Yu, J., Wu, S. & Wang, R. (2008). *Inorg. Chem.* **47**, 769–771.

# supporting information

*Acta Cryst.* (2018). E74, 949–954 [https://doi.org/10.1107/S2056989018008381]

## Crystal structure, Hirshfeld surface analysis and energy framework calculation of the first oxoanion salt containing 1,3-cyclohexanebis(methylammonium): [3-(azaniumylmethyl)cyclohexyl]methanaminium dinitrate

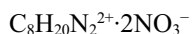
Hammouda Chebbi, Samia Mezrigui, Meriam Ben Jomaa and Mohamed Faouzi Zid

### Computing details

Data collection: CAD-4 EXPRESS (Duisenberg, 1992; Macíček & Yordanov, 1992); cell refinement: CAD-4 EXPRESS (Duisenberg, 1992; Macíček & Yordanov, 1992); data reduction: XCAD4 (Harms & Wocadlo, 1995); program(s) used to solve structure: SHELXS97 (Sheldrick, 2008); program(s) used to refine structure: SHELXL2014 (Sheldrick, 2015); molecular graphics: DIAMOND (Brandenburg, 2006) and Mercury (Macrae *et al.*, 2006); software used to prepare material for publication: WinGX (Farrugia, 2012) and publCIF (Westrip, 2010).

### [3-(Azaniumylmethyl)cyclohexyl]methanaminium dinitrate

#### Crystal data



$M_r = 268.28$

Orthorhombic,  $Pbca$

$a = 10.475$  (4) Å

$b = 16.884$  (4) Å

$c = 15.514$  (2) Å

$V = 2743.8$  (13) Å<sup>3</sup>

$Z = 8$

$F(000) = 1152$

$D_x = 1.299$  Mg m<sup>-3</sup>

Mo  $K\alpha$  radiation,  $\lambda = 0.71073$  Å

Cell parameters from 25 reflections

$\theta = 11\text{--}15^\circ$

$\mu = 0.11$  mm<sup>-1</sup>

$T = 293$  K

Plate, colorless

0.52 × 0.40 × 0.15 mm

#### Data collection

Enraf–Nonius CAD-4  
diffractometer

Radiation source: fine-focus sealed tube

Graphite monochromator

$\omega/2\theta$  scans

Absorption correction:  $\psi$  scan  
(North *et al.*, 1968)

$T_{\min} = 0.946$ ,  $T_{\max} = 1.000$

3798 measured reflections

2980 independent reflections

991 reflections with  $I > 2\sigma(I)$

$R_{\text{int}} = 0.036$

$\theta_{\max} = 27.0^\circ$ ,  $\theta_{\min} = 2.4^\circ$

$h = -13 \rightarrow 2$

$k = -1 \rightarrow 19$

$l = -1 \rightarrow 21$

2 standard reflections every 120 reflections  
intensity decay: 1%

#### Refinement

Refinement on  $F^2$

187 parameters

Least-squares matrix: full

0 restraints

$R[F^2 > 2\sigma(F^2)] = 0.062$

Hydrogen site location: mixed

$wR(F^2) = 0.173$

H atoms treated by a mixture of independent  
and constrained refinement

$S = 0.98$

2980 reflections

$$w = 1/[\sigma^2(F_o^2) + (0.063P)^2]$$

$$\text{where } P = (F_o^2 + 2F_c^2)/3$$

$$(\Delta/\sigma)_{\max} < 0.001$$

$$\Delta\rho_{\max} = 0.17 \text{ e \AA}^{-3}$$

$$\Delta\rho_{\min} = -0.13 \text{ e \AA}^{-3}$$

### Special details

**Geometry.** All esds (except the esd in the dihedral angle between two l.s. planes) are estimated using the full covariance matrix. The cell esds are taken into account individually in the estimation of esds in distances, angles and torsion angles; correlations between esds in cell parameters are only used when they are defined by crystal symmetry. An approximate (isotropic) treatment of cell esds is used for estimating esds involving l.s. planes.

**Refinement.** Refinement of  $F^2$  against ALL reflections. The weighted R-factor wR and goodness of fit S are based on  $F^2$ , conventional R-factors R are based on F, with F set to zero for negative  $F^2$ . The threshold expression of  $F^2 > 2\text{sigma}(F^2)$  is used only for calculating R-factors(gt) etc. and is not relevant to the choice of reflections for refinement. R-factors based on  $F^2$  are statistically about twice as large as those based on F, and R-factors based on ALL data will be even larger.

### Fractional atomic coordinates and isotropic or equivalent isotropic displacement parameters ( $\text{\AA}^2$ )

	<i>x</i>	<i>y</i>	<i>z</i>	$U_{\text{iso}}^*/U_{\text{eq}}$
N1	0.5381 (5)	0.0463 (2)	0.6598 (3)	0.0659 (10)
H1A	0.601 (4)	0.058 (2)	0.694 (3)	0.081 (16)*
H1B	0.550 (3)	0.080 (2)	0.611 (2)	0.085 (13)*
H1C	0.471 (4)	0.059 (3)	0.690 (3)	0.096 (19)*
N2	0.4634 (5)	-0.1776 (3)	1.0032 (3)	0.0674 (10)
H2D	0.534 (4)	-0.178 (3)	1.016 (3)	0.081 (19)*
H2E	0.431 (4)	-0.155 (2)	1.057 (3)	0.098 (15)*
H2F	0.426 (5)	-0.230 (3)	1.002 (3)	0.16 (2)*
C1	0.5681 (4)	-0.0935 (2)	0.7032 (2)	0.0606 (10)
H1	0.6549	-0.0819	0.7232	0.073*
C2	0.4800 (4)	-0.0856 (2)	0.7804 (2)	0.0652 (11)
H2A	0.4832	-0.0316	0.8016	0.078*
H2B	0.3930	-0.0965	0.7626	0.078*
C3	0.5166 (4)	-0.1416 (2)	0.8520 (2)	0.0601 (10)
H3	0.6037	-0.1279	0.8695	0.072*
C4	0.5197 (4)	-0.2269 (2)	0.8201 (2)	0.0652 (11)
H4A	0.5512	-0.2610	0.8657	0.078*
H4B	0.4338	-0.2437	0.8058	0.078*
C5	0.6040 (4)	-0.2355 (2)	0.7419 (2)	0.0784 (12)
H5A	0.6920	-0.2259	0.7583	0.094*
H5B	0.5979	-0.2893	0.7204	0.094*
C6	0.5673 (4)	-0.1791 (2)	0.6718 (2)	0.0741 (12)
H6A	0.4826	-0.1923	0.6510	0.089*
H6B	0.6264	-0.1845	0.6241	0.089*
C7	0.5393 (4)	-0.0372 (2)	0.6311 (2)	0.0701 (11)
H7A	0.6030	-0.0436	0.5862	0.084*
H7B	0.4568	-0.0503	0.6066	0.084*
C8	0.4321 (4)	-0.1278 (2)	0.9289 (2)	0.0710 (11)
H8A	0.4386	-0.0727	0.9458	0.085*
H8B	0.3442	-0.1377	0.9123	0.085*
N3	0.2781 (4)	-0.09045 (18)	0.1598 (2)	0.0718 (9)
O1	0.2195 (3)	-0.10116 (18)	0.0922 (2)	0.1032 (11)

O2	0.2248 (3)	-0.06216 (17)	0.22373 (18)	0.0826 (9)
O3	0.3922 (3)	-0.1097 (2)	0.16492 (19)	0.1031 (11)
N4	0.7872 (4)	-0.1535 (2)	0.0224 (2)	0.0685 (9)
O4	0.7259 (3)	-0.09475 (18)	0.0414 (3)	0.1171 (12)
O5	0.9065 (3)	-0.15214 (15)	0.02450 (17)	0.0747 (8)
O6	0.7335 (3)	-0.21487 (18)	0.0004 (2)	0.1000 (11)

*Atomic displacement parameters ( $\text{\AA}^2$ )*

	$U^{11}$	$U^{22}$	$U^{33}$	$U^{12}$	$U^{13}$	$U^{23}$
N1	0.070 (3)	0.063 (3)	0.065 (2)	-0.009 (2)	0.001 (3)	0.010 (2)
N2	0.071 (3)	0.078 (3)	0.054 (2)	0.000 (2)	0.001 (2)	0.0046 (19)
C1	0.064 (3)	0.059 (2)	0.058 (2)	-0.004 (2)	0.004 (2)	-0.001 (2)
C2	0.073 (3)	0.056 (2)	0.066 (2)	0.009 (2)	0.005 (2)	0.0013 (19)
C3	0.062 (2)	0.058 (2)	0.060 (2)	0.005 (2)	0.000 (2)	0.009 (2)
C4	0.072 (3)	0.054 (2)	0.069 (2)	0.003 (2)	0.000 (2)	0.0053 (19)
C5	0.098 (3)	0.058 (2)	0.080 (3)	0.013 (2)	0.011 (3)	-0.001 (2)
C6	0.091 (3)	0.062 (2)	0.070 (3)	0.003 (2)	0.016 (2)	0.000 (2)
C7	0.084 (3)	0.063 (3)	0.063 (2)	0.000 (2)	0.007 (2)	0.000 (2)
C8	0.076 (3)	0.071 (2)	0.066 (2)	0.012 (2)	0.007 (2)	0.007 (2)
N3	0.074 (3)	0.068 (2)	0.074 (3)	0.001 (2)	0.005 (2)	-0.0120 (19)
O1	0.092 (2)	0.140 (3)	0.078 (2)	0.009 (2)	-0.0104 (19)	-0.0334 (19)
O2	0.081 (2)	0.0903 (19)	0.0764 (18)	0.0065 (17)	0.0102 (17)	-0.0262 (16)
O3	0.074 (2)	0.140 (3)	0.096 (2)	0.028 (2)	-0.0052 (19)	-0.033 (2)
N4	0.070 (3)	0.075 (2)	0.060 (2)	-0.003 (2)	-0.016 (2)	0.0003 (19)
O4	0.091 (2)	0.095 (2)	0.165 (3)	0.024 (2)	-0.026 (2)	-0.042 (2)
O5	0.071 (2)	0.082 (2)	0.0709 (18)	-0.0077 (16)	-0.0064 (16)	-0.0090 (14)
O6	0.084 (2)	0.0728 (17)	0.143 (3)	-0.0103 (17)	-0.033 (2)	-0.0060 (18)

*Geometric parameters ( $\text{\AA}$ ,  $^\circ$ )*

N1—C7	1.479 (5)	C4—C5	1.507 (5)
N1—H1A	0.87 (4)	C4—H4A	0.9700
N1—H1B	0.95 (4)	C4—H4B	0.9700
N1—H1C	0.87 (5)	C5—C6	1.496 (5)
N2—C8	1.464 (5)	C5—H5A	0.9700
N2—H2D	0.77 (4)	C5—H5B	0.9700
N2—H2E	0.99 (4)	C6—H6A	0.9700
N2—H2F	0.96 (6)	C6—H6B	0.9700
C1—C7	1.499 (5)	C7—H7A	0.9700
C1—C2	1.518 (5)	C7—H7B	0.9700
C1—C6	1.524 (5)	C8—H8A	0.9700
C1—H1	0.9800	C8—H8B	0.9700
C2—C3	1.508 (4)	N3—O1	1.229 (4)
C2—H2A	0.9700	N3—O2	1.234 (4)
C2—H2B	0.9700	N3—O3	1.241 (4)
C3—C8	1.503 (5)	N4—O4	1.218 (4)
C3—C4	1.523 (5)	N4—O6	1.227 (4)

C3—H3	0.9800	N4—O5	1.250 (4)
C7—N1—H1A	113 (3)	C5—C4—H4B	109.3
C7—N1—H1B	109 (2)	C3—C4—H4B	109.3
H1A—N1—H1B	104 (3)	H4A—C4—H4B	108.0
C7—N1—H1C	114 (3)	C6—C5—C4	111.9 (3)
H1A—N1—H1C	103 (4)	C6—C5—H5A	109.2
H1B—N1—H1C	113 (4)	C4—C5—H5A	109.2
C8—N2—H2D	115 (3)	C6—C5—H5B	109.2
C8—N2—H2E	112 (2)	C4—C5—H5B	109.2
H2D—N2—H2E	96 (4)	H5A—C5—H5B	107.9
C8—N2—H2F	114 (3)	C5—C6—C1	111.7 (3)
H2D—N2—H2F	113 (5)	C5—C6—H6A	109.3
H2E—N2—H2F	104 (4)	C1—C6—H6A	109.3
C7—C1—C2	114.3 (3)	C5—C6—H6B	109.3
C7—C1—C6	111.2 (3)	C1—C6—H6B	109.3
C2—C1—C6	109.4 (3)	H6A—C6—H6B	107.9
C7—C1—H1	107.2	N1—C7—C1	112.4 (3)
C2—C1—H1	107.2	N1—C7—H7A	109.1
C6—C1—H1	107.2	C1—C7—H7A	109.1
C3—C2—C1	111.9 (3)	N1—C7—H7B	109.1
C3—C2—H2A	109.2	C1—C7—H7B	109.1
C1—C2—H2A	109.2	H7A—C7—H7B	107.9
C3—C2—H2B	109.2	N2—C8—C3	113.8 (3)
C1—C2—H2B	109.2	N2—C8—H8A	108.8
H2A—C2—H2B	107.9	C3—C8—H8A	108.8
C8—C3—C2	109.8 (3)	N2—C8—H8B	108.8
C8—C3—C4	114.6 (3)	C3—C8—H8B	108.8
C2—C3—C4	111.0 (3)	H8A—C8—H8B	107.7
C8—C3—H3	107.0	O1—N3—O2	121.1 (4)
C2—C3—H3	107.0	O1—N3—O3	119.8 (4)
C4—C3—H3	107.0	O2—N3—O3	119.1 (4)
C5—C4—C3	111.5 (3)	O4—N4—O6	120.9 (4)
C5—C4—H4A	109.3	O4—N4—O5	120.3 (4)
C3—C4—H4A	109.3	O6—N4—O5	118.8 (4)

*Hydrogen-bond geometry (Å, °)*

D—H···A	D—H	H···A	D···A	D—H···A
N1—H1A···O2 <sup>i</sup>	0.87 (4)	2.22 (4)	3.084 (6)	169 (4)
N1—H1A···O3 <sup>i</sup>	0.87 (4)	2.36 (4)	3.013 (5)	132 (3)
N1—H1B···O4 <sup>ii</sup>	0.95 (4)	2.59 (4)	3.187 (6)	121 (3)
N1—H1B···O5 <sup>ii</sup>	0.95 (4)	1.87 (4)	2.818 (5)	172 (3)
N1—H1C···O2 <sup>iii</sup>	0.87 (5)	2.12 (5)	2.939 (6)	157 (4)
N2—H2D···O4 <sup>iv</sup>	0.77 (4)	2.48 (4)	3.142 (6)	145 (4)
N2—H2D···O6 <sup>iv</sup>	0.77 (4)	2.19 (4)	2.899 (6)	153 (4)
N2—H2E···O1 <sup>iv</sup>	0.99 (4)	2.46 (4)	3.178 (6)	130 (3)
N2—H2E···O3 <sup>iv</sup>	0.99 (4)	1.88 (4)	2.858 (5)	173 (4)

---

N2—H2F···O5 <sup>v</sup>	0.96 (6)	2.05 (6)	2.967 (5)	159 (5)
N2—H2F···O6 <sup>v</sup>	0.96 (6)	2.23 (6)	3.016 (6)	139 (4)

---

Symmetry codes: (i)  $-x+1, -y, -z+1$ ; (ii)  $-x+3/2, -y, z+1/2$ ; (iii)  $-x+1/2, -y, z+1/2$ ; (iv)  $x, y, z+1$ ; (v)  $x-1/2, -y-1/2, -z+1$ .